1
2
3
4
5
6
7
8
9
10
11
12
13
14
15
16
17
18
19
20
21
22
23
24
25
26
27
28
29
30
31
32
33
34
35
36
37
38
39
40
41
42
43
44
45
46
47
48
49
50
51
52
53
54
55
56
57
58
59
60

Atomic layer deposited α-Ga_2O_3 solar-blind photodetectors

J. Moloney,[1†] O. Tesh,[1†] M. Singh,[2] J.W. Roberts,[3] J.C. Jarman,[1] L.C. Lee,[1] T.N. Huq,[1] J. Brister,[1] S. Karboyan,[2] M. Kuball,[2] P.R. Chalker,[3] R.A. Oliver,[1] and F.C-P. Massabuau[1*]

[1] *Department of Materials Science and Metallurgy, University of Cambridge, 27 Charles Babbage Road, Cambridge CB3 0FS, UK*

[2] *School of Physics, HH Wills Physics Laboratory, University of Bristol, Tyndall Avenue, Bristol BS8 1TL, UK*

[3] *School of Engineering, The University of Liverpool, Brownlow Hill, Liverpool L69 3GH, UK*

[†] These authors contributed equally to the work.

[*] Email: fm350@cam.ac.uk

Keywords

Gallium oxide, Ultraviolet, Photodetector, Atomic layer deposition, Anneal

Abstract

Low temperature atomic layer deposition was used to deposit α-Ga_2O_3 films, which were subsequently annealed at various temperatures and atmospheres. The α-Ga_2O_3 phase is stable up to 400 °C, which is also the temperature that yields the most intense and sharpest reflection by X-ray diffraction. Upon annealing at 450 °C and above, the material gradually turns into the more thermodynamically stable ε or β phase. The suitability of the materials for solar-blind photodetector applications has been demonstrated with the best responsivity achieved being 1.2 A/W under 240 nm illumination and 10 V bias, for the sample annealed at 400 °C in argon. It is worth noting however that the device performance strongly depends on the annealing conditions, with the device annealed in forming gas behaving poorly. Given that the tested devices have similar microstructure, the discrepancies in device performance are attributed to hydrogen impurities.

Introduction

Gallium oxide (Ga_2O_3) is currently viewed as one of the most promising wide band gap semiconductors for future power electronics and ultraviolet (UV) optoelectronics applications [1]. Currently, there are six reported Ga_2O_3 polymorphs, namely α, β, γ, δ, ε, and κ [2,3] – the κ phase being an ordered variant of the ε phase [4]. The monoclinic β phase is the only thermodynamically stable phase and has therefore been the focus of most research effort [1]. The rhombohedral α phase (corundum) is metastable and is therefore less studied, despite being the most promising polymorph for band gap engineering in the UV since it is isostructural with other group-III sesquioxide semiconductors (α-In_2O_3 and α-Al_2O_3) [5].

In the past, α-Ga_2O_3 has been stabilized under high pressures (several GPa) and high temperatures (1000 °C) [6,7]. More recently, stabilisation of this phase under less extreme conditions has been achieved, using mist chemical vapor deposition (CVD) at *ca.* 450 °C [5,8], metalorganic vapor phase deposition (MOCVD) at 600 °C [9], halide vapor phase epitaxy (HVPE) at 650 °C [10] and 550 °C

Accepted Manuscript

1 2 3 4 5 6 7 8 9 10 11 12 13 14 15 16 17 18 19 20 21 22 23 24 25 26 27 28 29 30 31 32 33 34 35 36 37 38 39 40 41 42 43 44 45 46 47 48 49 50 51 52 53 54 55 56 57 58 59 60

[11], molecular beam epitaxy (MBE) at 800-850 ºC [12], or RF magnetron sputtering at >600 ºC [13]. Using atomic layer deposition (ALD), most studies have reported the deposition of amorphous Ga_2O_3 films [14-20]. However, it has been recently demonstrated that α-Ga_2O_3 could also be synthesized using plasma-enhanced ALD at temperatures as low as 250 ºC [21]. To date, the body of work on this material has focused on growth aspects, and only a limited number of studies have reported the application of the grown materials in devices. In particular, for solar-blind UV detection applications (detection wavelength <280 nm) relatively few reports using α-Ga_2O_3 appear in the literature [12,22,23].

In an earlier paper, it was showed that *ca.* 130 nm thick films of α-Ga_2O_3 could be deposited by low temperature ALD on *c*-plane sapphire [21]. The films consisted predominantly of α phase columns. However, inclusions of the ε phase, as well as amorphous material, were also found. In the present study, it is shown that the quality of similarly grown films can be improved using post-deposition thermal annealing and the suitability of the resulting materials for solar-blind UV photodetector applications is demonstrated. A 3 orders of magnitude improvement of the device responsivity between the as-grown sample and the sample annealed in argon or oxygen at 400 ºC is reported, with the best device exhibiting a responsivity of *ca.* 1.2 A/W under 10 V bias and 240 nm illumination.

Methods

Deposition of Ga_2O_3 was achieved using alternating pulses of triethylgallium (TEGa) and O_2 plasma in an Oxford Instruments Plasma-OpAL ALD system. A *c*-plane sapphire substrate, with a miscut of 0.25±0.10º towards $(11\bar{2}0)$, was employed. The substrate temperature was set at 250 °C, reactor wall temperatures were 150 °C, the TEGa bubbler was kept at ~25 °C and the delivery lines from the TEGa bubbler to the deposition chamber were set at 50 °C. The base pressure in the chamber (with no process gases flowing) was *ca.* 10 mTorr. During the deposition processes the chamber pressure varied between *ca.* 80 mTorr (during the plasma steps) and 160 mTorr (during the TEGa dose). Each ALD cycle consisted of one 0.1 s pulse of TEGa with 100 sccm of Ar carrier gas, a 5 s purge using 100 sccm Ar through the TEGa line, a 5 s 300 W O_2 plasma exposure using 20 sccm O_2, and finally a 5 s purge using 100 sccm Ar. These conditions of temperature, plasma power and O_2 flow were found to be optimal for the growth of Ga_2O_3 in the α phase [24]. 2730 cycles were performed, resulting in a nominal film thickness of *ca.* 130 nm.

The samples were annealed after growth to improve the crystalline quality of the Ga_2O_3 films. Samples were placed on a flat bottom alumina boat and loaded into a clean quartz tube inside a small horizontal annealing furnace (Carbolite). The furnace temperature ramp rate was set to 10 °C/min using a Eurotherm temperature controller. The samples were annealed for 1 hour at various temperatures and atmospheres and were cooled down to room temperature before unloading. For the temperature series, the samples were annealed in air for 1 hour under 1000 mbar pressure, and temperatures of 300, 350, 400, 450, 500, 600 and 700 °C. For the ambient series, the samples were annealed for 1 hour under 1000 mbar pressure at 400 °C, and in atmospheres of argon, air, oxygen and forming gas (3% H_2, 97% N_2).

X-ray diffraction (XRD) was employed to investigate the phase and crystalline quality of the samples, as well as the strain state of the films. An X'pert MRD diffractometer, in open detector configuration (and using a 1º slit), was used to record symmetric 2θ-ω scans of the samples. The intensity of each spectrum has been normalized relative to the sapphire 0006 peak to avoid effects from illuminated area and variation in intensity of the X-ray source. A Panalytical Empyrean diffractometer with PIXcel detector was used to record reciprocal space maps (RSMs) of the symmetric 0006 and asymmetric $10\bar{1}10$ reflections (data not shown here).

Accepted Manuscript

1
2
3
4
5
6
7
8
9
10
11
12
13
14
15
16
17
18
19
20
21
22
23
24
25
26
27
28
29
30
31
32
33
34
35
36
37
38
39
40
41
42
43
44
45
46
47
48
49
50
51
52
53
54
55
56
57
58
59
60

Atomic force microscopy (AFM) was performed in peak force tapping mode using a Bruker Dimension Icon microscope. The peak force tapping yields a greater lateral resolution than other AFM techniques (*e.g.* intermittent-contact mode) due to the smaller tip radius (Bruker ScanAsyst-Air), which was nominally 2 nm.

Transmission electron microscopy (TEM) was used to observe the structure of the films in cross-section. High angle annular dark field scanning TEM (HAADF-STEM) was carried out in a FEI Tecnai Osiris operated at 200 kV.

Following cleaning in acetone and isopropyl alcohol, metal contacts were defined using UV lithography and thermal evaporation. Shipley s1813 positive photoresist was developed with MF-319, an aqueous developer containing dilute tetramethylammonium hydroxide (TMAH), after a short post-exposure treatment with chlorobenzene to produce the undercut profile required for the metal lift-off process. It was observed that the Ga_2O_3 film is slowly etched by the developer solution, and so care was taken to restrict the development time to the minimum required to clear the exposed areas. After resist processing, a 10 nm Ti adhesion layer and 80 nm Au were evaporated by resistive thermal evaporation from tungsten boats, and the patterns were lifted off in acetone. The devices were made of two interdigitated electrodes. The illuminated area of the devices is 0.425 mm^2.

The electrical properties of the devices were tested using a Keithley Source Measure Unit coupled with a probe station. To measure the optical response, a Xe lamp was used, which was spectrally filtered by a prism monochromator and controlled using LabView software. The optical fibre source was fixed at a distance of 2 cm from the device. To calibrate the setup, power output was measured at the same distance from the fibre and same wavelength used during the experiment. At 240 nm the input power density was 0.46 W/m^2. Dark current I-V curves were measured for all devices to ensure minimum current flow, followed by response measured at fixed 240 nm illumination (lamp ON time of 20 s and OFF time of 40 s has been fixed throughout the experiment).

Results and discussion

I. The impact of annealing at varying temperature

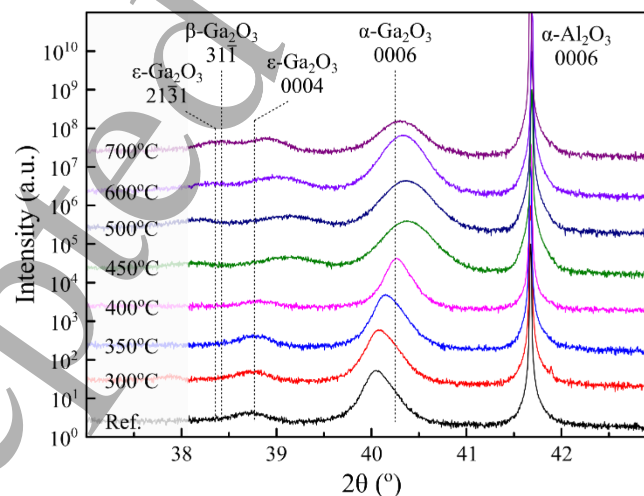

Figure 1 – Symmetric 2θ-ω scan for the samples annealed in air at various temperatures. The position of the reflections for the α, β and ϵ phases are obtained using the lattice parameters from Ref. [25], [26] and [4] respectively.

Figure 1 shows the symmetric 2θ-ω scan of the samples annealed in ambient air and at various temperatures. The 0006 reflection from the sapphire (α-Al_2O_3) substrate is clearly visible at 2θ =

Accepted Manuscript

1
2
3 41.68°. To facilitate interpretation, each spectrum has been normalized relative to the substrate peak. All the XRD diffractograms exhibit a 0006 reflection for α-Ga_2O_3 near 2θ = 40.25° (the expected value for a relaxed film, using the lattice parameter from Marezio *et al.* [25]). The peak shifts slightly depending on the annealing temperature – the origin of this shift will be discussed later. It can be seen from Figure 1 that the α phase is stable up to 400 °C. At this temperature, the 0006 reflection is the most intense and sharpest, which can be interpreted as an increase in crystalline quality of the film and/or an increase in crystallite size. Compared to the reference as-grown sample, annealing at 400 °C increases the 0006 peak intensity by a factor of 2-4.

For annealing temperatures above 450 °C, the α phase is still present in the film but the peak significantly broadens, and its intensity decreases, which is indicative of a poorer crystalline quality, smaller volume fraction of α phase and/or smaller crystallite size. Lee *et al.* reported that α-Ga_2O_3 grown by mist-CVD was stable up to 550 °C, beyond which temperature the material gradually transformed to β phase [27] – the present results are consistent with that study. It has been shown that doping the film with Al can be an effective approach to improve the stability of the α phase beyond 400 °C [28]. That is, however, beyond the scope of this work.

Additional peaks can be observed at lower 2θ values throughout the set of samples. In the reference sample, the peak at 2θ ~ 38.7° has previously been attributed to inclusions in the ϵ phase forming at the tip of the α-Ga_2O_3 columns [21]. A similar peak is observed in all the samples and it is also noted that this peak undergoes the same shift as the α-Ga_2O_3 0006 peak. For higher temperature anneals, an additional peak can be observed at lower 2θ value (at 2θ ~ 38.4°), which could be attributed to either ϵ-Ga_2O_3 $21\bar{3}1$ or β-Ga_2O_3 $31\bar{1}$ reflections – definitive identification is not possible. This peak gradually appears as the α-Ga_2O_3 0006 reflection weakens, supporting the idea that the α-phase decomposes to a thermodynamically more favourable phase, that is, ϵ or β [29].

The shift of the peaks towards higher 2θ angles with increasing annealing temperature could be attributed to several factors, such as change of strain in the film upon annealing, or interdiffusion of Ga with Al from the substrate (which has been reported by other studies despite the acknowledged chemical stability of sapphire [30-32]). From measurements of the *a* and *c* lattice parameters using RSM in the XRD, it is observed that the lattice parameters are inversely correlated, *i.e.* an increase in the *c* parameter is associated with a decreasing *a* parameter. Consequently, the volume of the unit cell remains relatively constant (all values are within a 1% relative range) throughout the set of samples. This is a strong indication that the peak shift is strain-induced rather than composition-induced. Indeed, if the film was being contaminated with Al by interdiffusion from the substrate, we would expect (i) a decrease of the unit cell volume associated with the peak shift, and (ii) a continuous shift of the peak towards higher angles as the annealing temperature increases (instead, the peak stops shifting for temperatures above 450 °C).

Accepted Manuscript

1 2 3 4 5 6 7 8 9 10 11 12 13 14 15 16 17 18 19 20 21 22 23 24 25 26 27 28 29 30 31 32 33 34 35 36 37 38 39 40 41 42 43 44 45 46 47 48 49 50 51 52 53 54 55 56 57 58 59 60

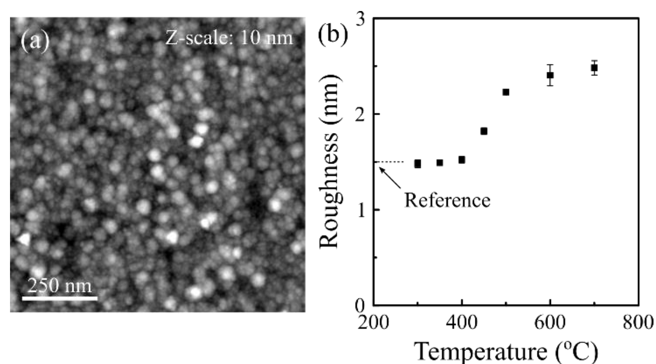

Figure 2 – (a) Typical AFM topography image of the samples (here the sample annealed at 400 °C). (b) RMS roughess of the samples annealed in air at various temperatures. The roughness was obtained from 1 µm x 1 µm AFM images.

The topography of all the samples has been investigated using AFM. All the samples exhibited a similar morphology, as shown in Figure 2(a). It is noted however that the annealing temperature effects the height range of the sample, but not visibly the lateral dimensions of the features. The evolution of the root mean square (RMS) roughness over a 1 µm x 1 µm area with annealing temperature is shown in Figure 2(b). In particular, a roughening of the surface for temperatures above 400 °C is observed, which correlates with the decrease of the α phase peak in the XRD diffractograms (Figure 1). A power spectral density analysis of the AFM data provides further insights on the mechanisms dominating the topography. Following the approach described in Refs. [33,34], the dominant smoothing (plastic flow, evaporation/recondensation, bulk diffusion, or surface diffusion) and roughening (stochastic or non-stochastic) mechanisms in films during growth, annealing or etching could be determined. It was found that the dominant smoothing mechanism in all the samples is by surface diffusion (the power law gradient ranges between 3.9 and 4.4) while roughening tends to be stochastic. This may imply that upon annealing, material is lost from random positions across the surface (stochastic roughening) while surface migration of atoms occurs to smoothen the topography. The overall increase in roughness with annealing temperature indicates that, whilst smoothing and roughening processes are competing to results in the observed topography, the (stochastic) roughening tend to dominate during annealing.

II. The impact of annealing under different atmospheres

Accepted Manuscript

1 2 3 4 5 6 7 8 9 10 11 12 13 14 15 16 17 18 19 20 21 22 23 24 25 26 27 28 29 30 31 32 33 34 35 36 37 38 39 40 41 42 43 44 45 46 47 48 49 50 51 52 53 54 55 56 57 58 59 60

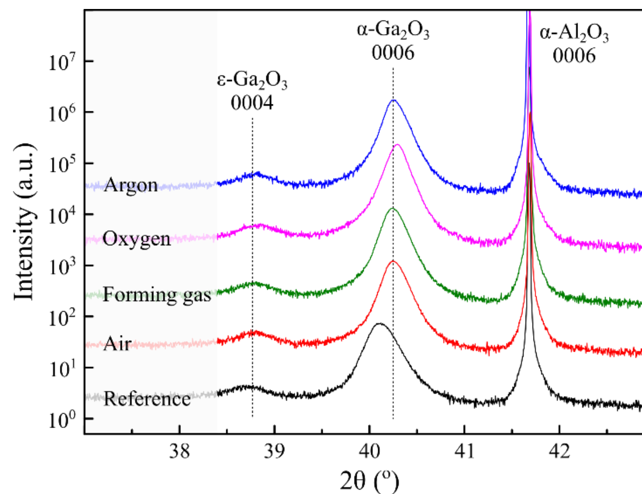

Figure 3 – Symmetric 2θ-ω scan for the samples annealed at 400 °C in various atmospheres. The position of the reflections for the α and ϵ phases are obtained using the lattice parameters from Ref. [25] and [4] respectively.

It was established earlier that 400 °C was the optimal annealing temperature in air – leading to the sharpest and most intense α-Ga_2O_3 reflection. Figure 3 presents the XRD diffratograms of the samples annealed at 400 °C under different atmospheres – *i.e.* air, argon, oxygen, and forming gas (3% H_2, 97% N_2). Firstly, all these annealed samples show a sharper and more intense α-Ga_2O_3 0006 reflection compared to the reference sample (the scans are normalized to the substrate reflection): the samples annealed in air, argon and forming gas exhibit approximately a 2-fold increase in peak intensity relative to the as-grown sample, while the sample annealed under oxygen shows a 3-fold improvement. It is also noted that the peaks all shift to the same value in 2θ indicating that all the films have the same strain state irrespective of the ambient employed. The topography of the samples grown under different anneals was also analysed using AFM (data not shown). All the data obtained were similar to the image presented in Figure 2(b), with a roughness of *ca.* 1.3 nm for all the samples. It is concluded that, as far as the AFM and XRD data are concerned, the annealing temperature has a much greater impact on the film structural properties than the annealing atmosphere.

III. Solar-blind photodetector devices

Metal-Semiconductor-Metal (MSM) photodetectors were subsequently fabricated from the reference as-grown sample and the samples annealed at 400 °C under different atmospheres. The devices' main characteristics are listed in Table 1, together with those from similar MSM device structures from the literature.

Sample	Responsivity (A/W) at 240 nm	Dark current (pA)	$(I_{photo}-I_{dark})/I_{dark}$
Reference	3.1×10^{-4} (± 0.1×10^{-4})	0.2	~4.5×10^{2}
Air	4.8×10^{-1} (± 0.1×10^{-1})	3	~3.5×10^{4}
Forming gas	1.2×10^{-2} (± 0.1×10^{-2})	19	~1.5×10^{2}
Oxygen	1.038 (± 0.004)	8	~2.5×10^{4}
Argon	1.17 (± 0.01)	163	~1.5×10^{3}
Guo *et al.* [12]	0.007 (10V; 254 nm)	1020	30-68
Lee *et al.* [22]	0.76 (20V; 253 nm)	0.5	~10^{4}

Table 1 – Summary of device performances: responsivity at 240 nm illumination and 10 V bias; dark current recorded at 10 V bias; photo-to-dark current contrast.

Accepted Manuscript

1
2
3
4
5
6
7
8
9
10
11
12
13
14
15
16
17
18
19
20
21
22
23
24
25
26
27
28
29
30
31
32
33
34
35
36
37
38
39
40
41
42
43
44
45
46
47
48
49
50
51
52
53
54
55
56
57
58
59
60

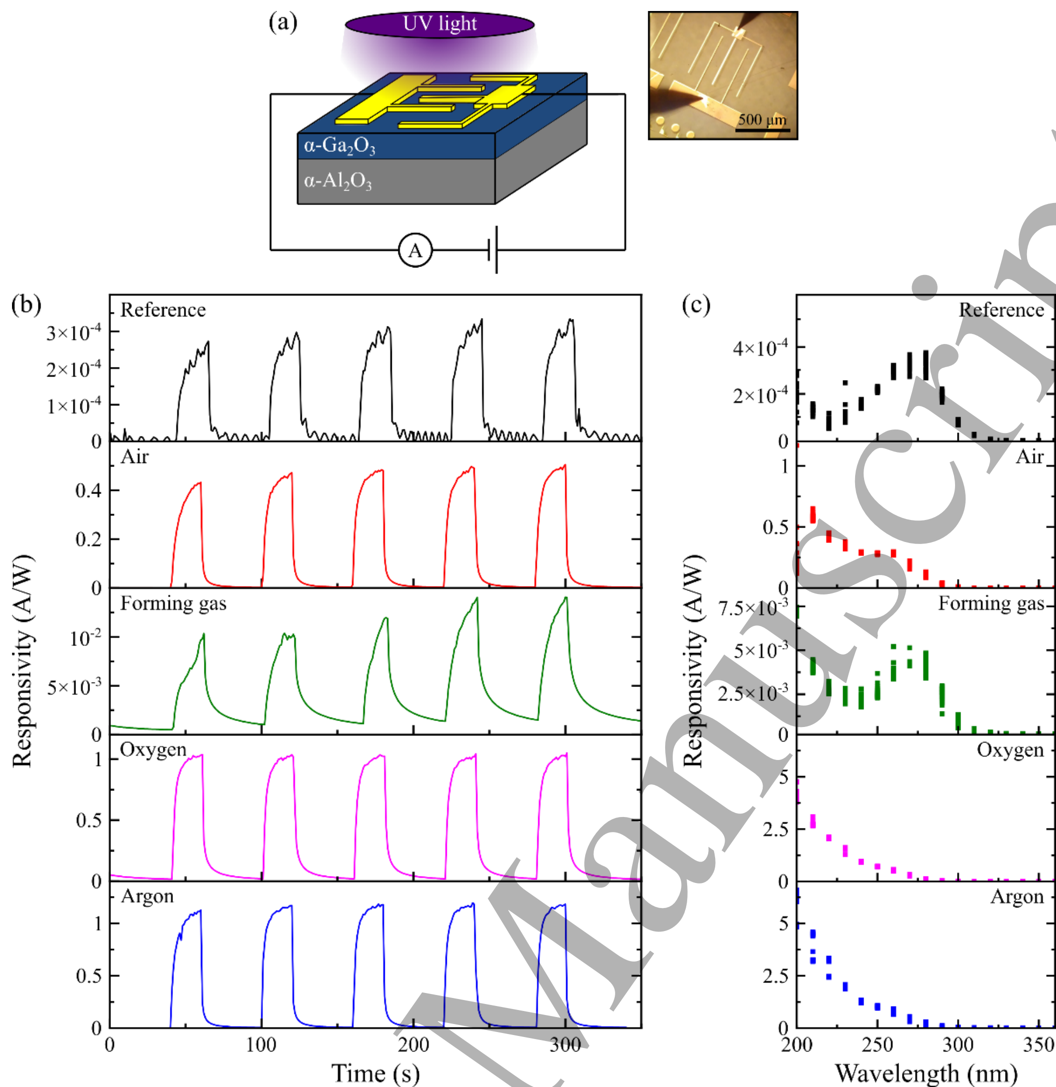

Figure 4 – (a) Schematic of the device testing setup. (b) Responsivity of the devices tested under illumination of 240 nm (power density 0.46 $W.m^{-2}$) and 10 V bias. The light source was turned ON for 20 s and OFF for 40 s. (c) Spectral response of the devices illuminated under wavelength from 200 to 360 nm and 10 V bias.

The optical response of the devices recorded under 240 nm UV illumination and 10 V bias, is shown in Figure 4(a). A clear increase in photocurrent can be observed when the devices are illuminated under 240 nm – *i.e.* near the optical bandgap of α-Ga_2O_3 [5,9,17]. The dark current varies between samples, but overall remains fairly low – of the order of a few pA. The photo-to-dark current contrast varies between samples from *ca.* 1.5 $x10^2$ to up to *ca.* 3.5 $x10^4$ depending on the annealing conditions, which demonstrates a good photoconductive behaviour. It is noted however that the devices are relatively slow in response. The rise and decay times in all the devices are of the order of several seconds. This is clearly a point that needs to be addressed in future devices.

The responsivity of the as-grown sample is rather low, at 0.3 mA/W, but increases significantly by about 3 orders of magnitudes upon annealing. For anneals in argon and oxygen, the responsivity at 240 nm illumination and 10 V bias is *ca.* 1.2 and 1 A/W, respectively, which to our knowledge, is the best performance reported for α-Ga_2O_3 MSM photodetectors so far (note that direct comparison is difficult, as the other reported results used different illumination and/or bias conditions). To put these results into a broader context, photodetectors made from Ga_2O_3 phases that have received more

Accepted Manuscript

1 2 3 4 5 6 7 8 9 10 11 12 13 14 15 16 17 18 19 20 21 22 23 24 25 26 27 28 29 30 31 32 33 34 35 36 37 38 39 40 41 42 43 44 45 46 47 48 49 50 51 52 53 54 55 56 57 58 59 60

research effort exhibit responsivities such as 45.11 A/W (under 253 nm and 20 V conditions) for amorphous Ga_2O_3 [35], and 96.13 A/W (under 250 nm and 5 V conditions) for β-Ga_2O_3 [36].

The spectral response of the devices, shown in Figure 4(b), demonstrates the suitability of all the devices to detect radiations in the solar-blind region. The responsivity is very low in the long wavelength side (*i.e.* for sub-bandgap excitation). A peak in response can be seen for all samples for approximately 260-280 nm illumination (this peak is more or less pronounced between the samples) and corresponds to transitions across the bandgap of α-Ga_2O_3. It is worth noting that this corresponds to a slightly lower energy transition than the expected bandgap [5,9,24], which may imply the presence of shallow states near the band edges. The short wavelength response links to near surface photoconduction, which appears to be enhanced in the case of anneals in argon and oxygen compared to the other samples [37].

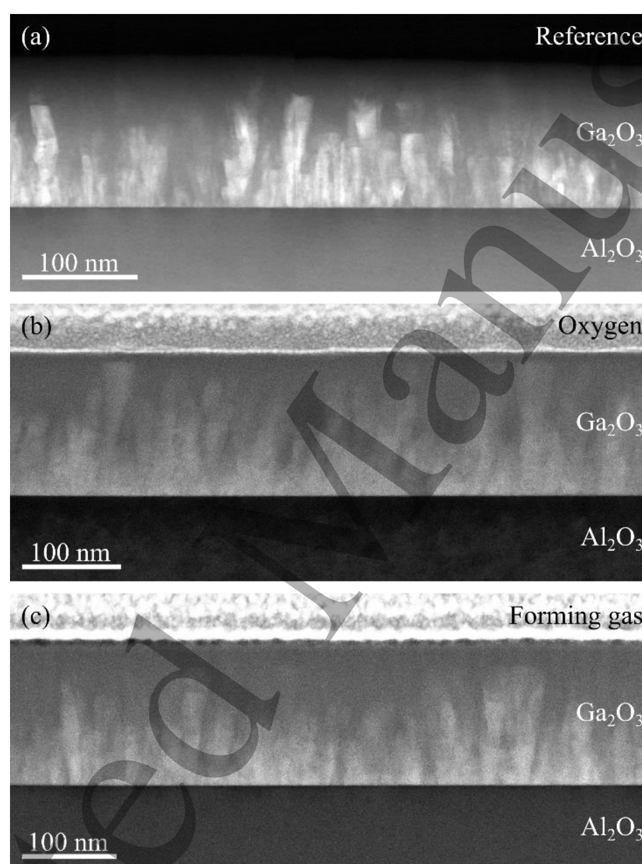

Figure 5 – HAADF-STEM images of (a) the as-deposited sample, (b) the sample annealed in oxygen at 400 °C, and (c) the sample annealed in forming gas at 400 °C.

Finally, we point out that the sample annealed in forming gas behaves surprisingly poorly compared to the other annealed samples. The responsivity of this device is about 2 orders of magnitude below the other annealed samples and the rise and decay times are significantly longer (the photocurrent does not reach saturation within the 20 s illumination window) (Figure 4(a)). Figure 4(b) also shows that this sample has almost no photoresponse for short wavelength illumination. To better understand the origin of this variation, TEM imaging of the as-grown sample, of the sample annealed in oxygen, and of the forming gas annealed sample was conducted. As illustrated in Figure 5, all three samples are nearly identical; they exhibit a columnar structure of α-Ga_2O_3 separated by amorphous Ga_2O_3 [21] and the columns have visually similar width and height. It appears that all the annealed samples

Accepted Manuscript

exhibit a columnar structure (from TEM observations); a comparable α phase volume fraction or crystallite size (from XRD 2θ-ω scans); and similar strain state (from XRD RSMs). The reason for the lower responsivity of the device annealed in forming gas does not appear to derive from the microstructure of the film. Given that only the sample annealed in forming gas – from a sample set that includes air, oxygen, argon and forming gas atmosphere – behaves poorly, we tentatively attribute this to hydrogen impurities in the film. This is a reasonable suggestion given that the extremely long rise and decay time of the forming gas device imply the presence of trap states in the film (this comment could also be made for the reference sample, although it is impossible to hold a specific point defect responsible in that case). In β-Ga_2O_3, hydrogen has been predicted to act as a shallow donor [38] and hydrogen termination at the sample surface has been shown to strongly affect the electron density and band bending at the sample surface [39,40]. However, the behaviour of hydrogen could differ significantly depending on the oxide material under consideration [41], and a proper study of the impact of hydrogen in specifically α-Ga_2O_3 materials would be necessary.

Conclusion

In conclusion, α-Ga_2O_3 has been deposited by low-temperature ALD and the film quality has been improved using post-deposition anneals at temperatures up to 400 ºC and atmospheres. The α-Ga_2O_3 films are stable up to 400 ºC, which is also the temperature that yields the most intense and sharpest XRD reflection. The suitability of the materials for solar-blind photodetector applications has been demonstrated with best responsivity of 1.2 A/W under 240 nm illumination and 10 V bias reported for the sample annealed at 400 ºC in an argon atmosphere. It is finally noted that better control over impurities in the materials could lead to further improvements in device performance.

Acknowledgements

This project is funded by the Engineering and Physical Sciences Research Council (EPSRC Grants No. EP/P00945X/1, EP/M010589/1 and EP/K014471/1). T.N.H. acknowledges funding from the EPSRC Centre for Doctoral Training in Graphene Technology (Grant No. EP/L016087/1).

References

[1] Pearton SJ, Yang J, Cary IV PH, Ren F, Kim J, Tadjer MJ and Mastro MA 2018 *Appl. Phys. Rev.* **5** 011301

[2] Roy R, Hill VG and Osborn EF 1952 *J. Am. Chem. Soc.* **75** 719

[3] Playford HY, Hannon AC, Barney ER and Walton RI 2013 *Chem. Eur. J.* **19** 2803

[4] Cora I, Mezzadri F, Boschi F, Bosi M, Caplovicova M, Calestani G, Dodony I, Pecz B and Fornari R 2017 *CrystEngComm* **19** 1509

[5] Fujita S and Kaneko K 2014 *J. Cryst. Growth* **401** 588

[6] Remeika JP and Marezio M 1966 *Appl. Phys. Lett.* **8** 87

[7] Machon D, McMillan PF, Xu B and Dong J 2006 *Phys. Rev. B* **73** 094125

[8] Sinohara D and Fujita S 2008 *Jap. J. Appl. Phys.* **47** 7311

[9] Sun H, Li KH, Torres Castanedo CG, Okur S, Tompa GS, Salagaj T, Lopatin S, Genovese A and Li X 2018 *Cryst. Growth Des.* **18** 2370

Accepted Manuscript

1
2
3
4
5
6
7
8
9
10
11
12
13
14
15
16
17
18
19
20
21
22
23
24
25
26
27
28
29
30
31
32
33
34
35
36
37
38
39
40
41
42
43
44
45
46
47
48
49
50
51
52
53
54
55
56
57
58
59
60

[10] Yao Y, Okur S, Lyle LAM, Tompa CS, Salagaj T, Sbrockey N, Davis RF and Porter LM 2018 *Mater. Res. Lett.* **6** 268

[11] Leach JH, Udwary K, Rumsey J, Dodson G, Splawn H, and Evans KR 2018 *APL Mater.* **7** 022504

[12] Guo DY, Zhao XL, Zhi YS, Cui W, Huang YQ, An YH, Li PG, Wu ZP, and Tang WH 2016 *Mat. Lett.* **164** 364

[13] Akazawa H 2016 *Vacuum* **123** 8

[14] Comstock DJ and Elam JW 2012 *Chem. Mater.* **24** 4011

[15] Shih HY, Chu FC, Das A, Lee CY, Chen MJ and Lin RM 2016 *Nanoscale Res. Lett.* **11** 235

[16] Donmez I, Ozgit-Akgun C and Biyikli N 2013 *J. Vac. Sci. Technol. A* **31** 01A110

[17] Choi DW, Chung KB and Park JS 2013 *Thin Solid Films* **546** 31

[18] Dezelah CL, Niinisto J, Arstila K, Niinisto L and Winter CH 2006 *Chem. Mater.* **18** 471

[19] O'Donoghue R, Rechmann J, Aghaee M, Rogalla D and Beck HW 2017 *Dalton Trans.* **46** 16551

[20] Li X, Lu H-L, Ma H-P, Yang J-G, Chen J-X, Huang W, Guo Q, Feng J-J and Zhang DW 2019 *Cur. Appl. Phys.* **19** 72

[21] Roberts JW, Jarman JC, Johnstone DN, Midgley PA, Chalker PR, Oliver RA and Massabuau FCP 2018 *J. Cryst. Growth* **487** 23

[22] Lee SH, Lee KM, Kim YB, Moon YJ, Kim SB, Bae D, Kim TJ, Kim YD, Kim SK and Lee SW 2019 *J. Alloys and Compounds* **780** 400

[23] Chen X, Xu Y, Zhou D, Yang S, Ren F, Lu H, Tang K, Gu S, Zhang R, Zheng Y and Ye J 2017 *ACS Appl. Mater. Interfaces* **9** 36997

[24] Roberts JW, Chalker PR, Ding B, Oliver RA, Gibbon JT, Jones L, Dhanak VR, Phillips LJ, Major J and F.C-P. Massabuau Low temperature growth and optical properties of α-Ga_2O_3 deposited on sapphire by plasma enhanced atomic layer deposition (in preparation)

[25] Marezio M and Remeika JP 1966 *J. Chem. Phys.* **46** 1862

[26] Ahman J, Svensson G and Albertsson 1996 *Acta Cryst. Sect. C***52** 1336

[27] Lee SD, Akaiwa K and Fujita S 2013 *Phys. Status Solidi C* **10** 1592

[28] Lee SD, Ito Y, Kaneko K and Fujita S 2015 *Jap. J. Appl. Physics* **54**, 030301

[29] Yoshioka S, Hayashi H, Kuwabara A, Oba F, Matsunaga K and Tanaka I 2007 *J. Phys.: Condens. Matter* **19** 346211

[30] Rogers DJ, Bove P, Arrateig X, Sandana VE, Teherani FH, Razeghi M, McClintock R, Frisch E and Harel S 2018 *Proc. SPIE* **10533** 105331P

[31] Rogers DJ, Look DC, Hosseini Téhérani F, Minder K, Razeghi M, Largeteau A, Demazeau G, Morrod J, Prior KA, Lusson A and Hassani S 2008 *Phys. Status Solidi C* **5** 3084

Accepted Manuscript

[32] Goyal A, Yadav BS, Thakur OP and Kapoor AK, Structural and Optical Characterization of β-Ga_2O_3 Thin Films Grown by Pulsed Laser Deposition. In: Jain V., Verma A. (eds) Physics of Semiconductor Devices. Environmental Science and Engineering (2014). Springer, Cham

[33] Koleske DD, Coltrin ME, Cross KC, Mitchell CC and Alleman AA 2004 *J. Cryst. Growth* **273** 86

[34] Oliver RA, Sumner J, Kappers MJ and Humphreys CJ 2009 *J. Appl. Phys.* **106** 054319

[35] Lee SH, Kim SB, Moon Y-J, Kim SM, Jung HJ, Seo MS, Lee KM, Kim S-K and Lee SW 2017 *ACS Photonics* **4** 2937

[36] Arora K, Goel N, Kumar M and Kumar M 2018 *ACS Photonics* **5** 2391

[37] Sze SM 1985 *Semiconductor Devices - Physics and Technology* (New York: Wiley)

[38] Varley JB, Weber JR, Janotti A and Van de Walle CG 2010 *Appl. Phys. Lett.* **97** 142106

[39] Swallow JEN, Varley JB, Jones LAH, Gibbon JT, Piper LFJ, Dhanak VR and Veal TD 2019 *APL Mater.* **7** 022528

[40] Polyakov AY, Lee IH, Smirnov NB, Yakimov EB, Shchemerov IV, Chernykh AV, Kochkova AI, Vasilev AA, Ren F, Carey IV PH and Pearton SJ 2019 *Appl. Phys. Lett.* **115** 032101

[41] Stavola M, Bekisli F, Yin W, Smithe K, Beall Fowler W and Boatner LA 2014 *J. Appl. Phys.* **115** 012001

Accepted Manuscript